important to estimate the errors introduced using segmented electrodes in measuring local mass transfer rates.

Acknowledgement—The authors are indebted to the Korea Science and Engineering Foundation (KOSEF) for partial support of this research.

REFERENCES

1. C. S. Lin, E. B. Denton, H. S. Gaskill and G. L. Putnam, Diffusion-controlled electrode reactions, *Ind. Engng Chem.* **43,** 2136–2143 (1951).
2. L. P. Reiss and T. J. Hanratty, Measurement of instantaneous rates of mass transfer to a small sink on a wall, *A.I.Ch.E. Jl* **8,** 245–247 (1962).
3. P. P. Grassman, Application of the electrolytic method—I. Advantages and disadvantages, mass transfer between a falling film and the wall, *Int. J. Heat Mass Transfer* **22,** 795–798 (1979).
4. D. J. Tagg, M. A. Patrick and A. A. Wragg, Heat and mass transfer downstream of abrupt nozzle expansions in turbulent flow, *Trans. Instn Chem. Engrs* **57,** 176–181 (1979).
5. A. A. Wragg, D. J. Tagg and M. A. Patrick, Diffusion controlled current distributions near cell entries and corners, *J. Appl. Electrochem.* **10,** 43–47 (1980).
6. J. K. Aggarwal and L. Talbot, Electro-chemical measurements of mass transfer in semi-cylindrical hollows, *Int. J. Heat Mass Transfer* **22,** 61–75 (1979).
7. P. H. Bradley, J. L. Greatorex and F. B. Leitz, Effect of turbulence promoters on local mass transfer, OSW contract No. 14-01-0001-2174 (1970).
8. D. H. Kim, I. H. Kim and H. N. Chang, Experimental study of mass transfer around a turbulence promoter by the limiting current method, *Int. J. Heat Mass Transfer* **26,** 1007–1016 (1983).
9. W. F. Ames, *Numerical Methods for Partial Differential Equations.* Academic Press, New York (1977).

Int. J. Heat Mass Transfer. Vol. 27, No. 10, pp. 1925–1928, 1984
Printed in Great Britain

0017–9310/84 $3.00 + 0.00

Non-uniform energy generation effects on natural convection in a spherical annulus enclosure

J. M. NELSEN† and R. W. DOUGLASS

Department of Mechanical Engineering, University of Nebraska, Lincoln, NE 68588-0525, U.S.A.

(*Received* 7 *February* 1983 *and in revised form* 10 *January* 1984)

NOMENCLATURE

$f(r)$ dimensionless generation rate function
g gravitational acceleration [m s^{-2}]
Gr Grashof number, $g\beta R_2^5\bar{Q}/kv^2$
k thermal conductivity of the fluid [W m^{-1} K^{-1}]
Pr Prandtl number, v/α
$q_w(\theta)$ local wall heat flux, $q_w^*/(R_2\bar{Q}) = (\partial T/\partial r)_1$ [W m^{-2}]
$\dot{q}(r)$ prescribed energy generation rate function, $\dot{Q}f(r)$ [W m^{-3}]
$\dot{Q}$ maximum value of $\dot{q}(r)$ [W m^{-3}]
$\bar{Q}$ volume averaged rate of energy released,

$$\frac{3\dot{Q}}{(1-\eta^3)}\int_\eta^1 f(r)r^2\,dr\ [\mathrm{W\,m^{-3}}]$$

r radial coordinate [m]
R_1, R_2 inner and outer sphere radii [m]
$T(r,\theta)$ temperature field [K]
T_2 outer sphere temperature.

Greek symbols
α thermal diffusivity of the fluid [m^2 s^{-1}]
β coefficient of volume expansion of the fluid [K^{-1}]
η radius ratio, R_1/R_2
θ latitudinal coordinate
v kinematic viscosity of the fluid [m^2 s^{-1}]
$\psi(r,\theta)$ stream function [m^3 s^{-1}].

Subscripts
$(\,)_r$ partial derivative with respect to r

Superscripts
$(\,)^*$ dimensional quantity.

INTRODUCTION

IN A RECENT paper Nelsen *et al.* [1] discussed natural convection in a spherical annulus driven by uniformly distributed energy generation within the annulus fluid. The purpose of this note is to extend those results to include radially non-uniform generation rate distributions in the annulus and to investigate their effect on the flow field. Under study is the steady buoyancy driven flow of a Boussinesq fluid within a concentric spherical annulus enclosure. The inner wall is insulated while the outer sphere is an isotherm (T_2). Such a configuration is of practical interest as discussed in ref. [1]. Of interest here, however, are the generic attributes of the apparatus as determined by an approximate numerical method, the method of partial spectral expansions.

MATHEMATICAL MODEL AND SOLUTION

A Boussinesq fluid fills a concentric spherical annulus enclosure whose inner radius is R_1 and outer radius is R_2. The fluid is generating energy at a prescribed rate, $\dot{q} = \dot{q}(r)$.

† Present address: Sandia National Laboratories, Albuquerque, NM 87185, U.S.A.

Table 1. Generation rate distributions giving $\bar{Q} = 1$ W m^{-3}

Profile name	$\dot{q}^* = \dot{Q}f(r)$ [W m^{-3}]
CON	1
SIN	$1.59554 \sin[\pi(r-\eta)/(1-\eta)]$
LPS	$1.64706(r-\eta)/(1-\eta)$

Spherical coordinates are used and axisymmetry is assumed. The axis is defined as a line parallel to the gravitational vector passing through the spheres' centers. The latitudinal coordinate, θ, is measured from the top or 'north pole'. The solution is valid in a domain: $\eta \leqslant r \leqslant 1$ and $0 \leqslant \theta \leqslant \pi$.

The governing system of equations is formulated in terms of the dimensionless stream function, $\psi(r, \theta)$, and temperature field, $T(r, \theta)$, as in refs. [2, 3] (with $\lambda = 1$) and are not listed here. The dimensionless variables are related to the physical quantities (with asterisks) as: $r^* = R_2 r$, $\psi^* = R_2 \nu \psi$, $T^* = (R_2^2 \bar{Q}/k)T + T_2$, and $\dot{q}^*(r) \equiv \dot{Q}f(r) = \bar{Q}q(r)$. The flow conditions are no-slip and no-cross-flow at solid surfaces. The thermal conditions are given as $T_r(\eta, \theta) = T(1, \theta) = 0$. The generation rate profiles used are summarized in Table 1.

$\dot{Q}$ has been chosen so that $\bar{Q}$ is the same for each profile: 1 W m^{-3}. The Grashof number, being defined in terms of $\bar{Q}$, does not change value. Each shape for $\dot{q}$ has the same thermal potential but it is distributed differently within each profile chosen. Note that for $\eta = 0.5$, $\bar{Q}_{SIN} = 0.6268\dot{Q}$ and $\bar{Q}_{LPS} = 0.6071\dot{Q}$.

The governing system of equations is solved by an approximate solution method known as partial spectral expansions. Specific information about the method and its convergence may be found in ref. [3].

RESULTS AND DISCUSSION

The flow field determined by the stream function and temperature distribution depends upon the spatial co-ordinates, the dimensionless parameters of the problem, and the shape of the generation function. That is

$$\psi, T = \psi, T(r, \theta; \eta, Gr, Pr; \dot{q}).$$

In this paper the radius ratio is fixed at $\eta = 0.5$, the Prandtl number at $Pr = 1.0$, and the Grashof number at $Gr = 10^7$.

Being insulated, the inner sphere will be warmer than the outer. Thus, natural convection will be established with upward flow along the inner sphere and downward along the outer. The streamlines should generally show a clockwise circulation pattern with the magnitude and shape dependent upon the particular generation profile used. Note that with the boundary conditions of this problem, if $\dot{q} = 0$, there is no flow and the fluid is uniform at T_2.

These effects are illustrated in Figs. 1 and 2 which show isotherm and streamline contours, respectively. In spite of the distinctly different generation rate profiles used, the isotherms of Fig. 1 show a rather similar shape. In each case, the upper latitudes are nearly twice as warm as the lower latitudes with the warmest spots lying on the north polar axis. The isotherm magnitudes do show a significant change with profile shape. Note that 'CON' results may be seen in Fig. 3 of ref. [1], p. 174 and that, in this case, $T_{max} = 0.03174$.

Regarding the streamline contours shown in Fig. 2, only results from the SIN and LPS cases are shown. The contour shapes are not strongly dependent on the generation rate profile. Magnitudes, however, do vary with the LPS profile having the smaller values of ψ. Note that for CON, $\psi_{max} = 15.64$. It is confirmed in Fig. 2 that any generation rate profile which has a maximum near the inner sphere will abet the natural circulation. Conversely, those profiles which peak near the outer sphere will tend to retard the flow.

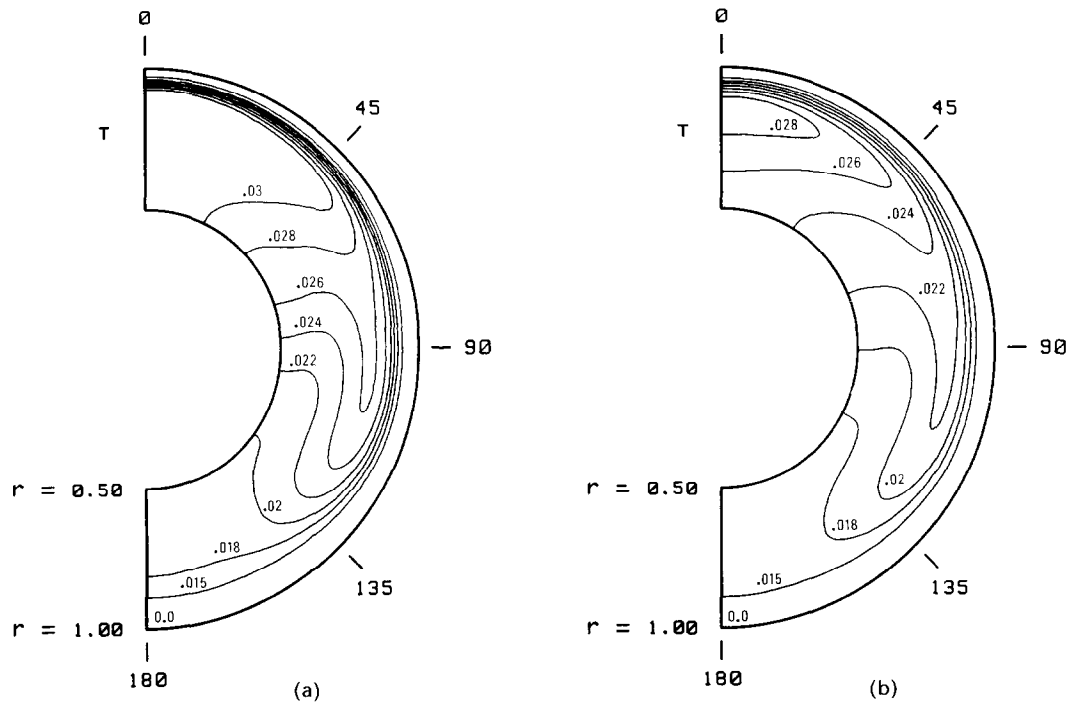

FIG. 1. Isotherm contour maps for $\eta = 0.5$, $Pr = 1.0$, and $Gr = 10^7$ with the inner sphere insulated and the outer maintained at $T_2 = 0$ showing the effect of non-uniform energy generation rates: (a) SIN; and (b) LPS. The dependent variable $T(r, \theta)$ is shown.

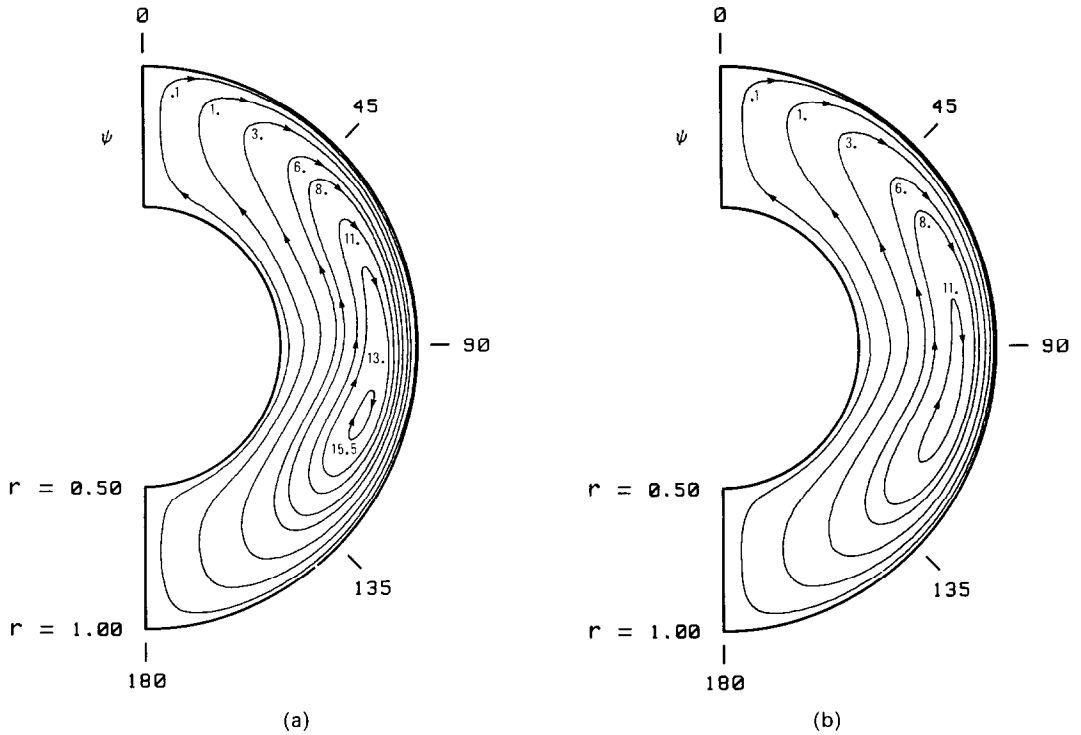

FIG. 2. Streamline contour maps showing the effect of non-uniform energy generation rates for the same conditions specified in Fig. 1: (a) SIN; and (b) LPS. The dependent variable $\psi(r, \theta)$ is shown.

Of final concern is the local heat flux along the outer sphere and the inner sphere's temperature. The inner sphere being insulated has no energy transported across it. All energy must cross the outer sphere. Thus, an integrated heat flux across the outer surface simply gives an energy balance, nothing more. Figure 3 shows both of these results for the cases discussed above. The area contained between the q_w curves and the line $q_w = 0$ is proportional to the total integrated rate of energy generated, a constant here. The curves show in each case that the largest rate of energy transport occurs at the top of the outer sphere, decreasing to a minimum flux at the bottom. Additionally, the inner sphere is always warmest near the top with the SIN profile consistently giving the warmest inner sphere and the LPS profile the coolest. This is not surprising since the LPS profile concentrates the energy release at the outer sphere, while SIN peaks nearer to the inner surface.

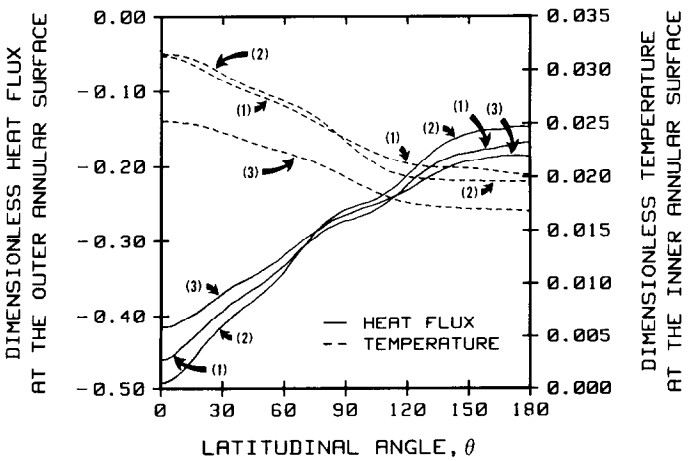

FIG. 3. Local outer sphere heat flux and inner sphere temperature ($T(\eta, \theta)$) results for the same conditions as used in Fig. 1. Note that $q_w < 0$ refers to energy leaving the annulus and that (1) = CON, (2) = SIN, (3) = LPS.

CONCLUSIONS

Based on the data presented herein, for a selected set of parameters, it is determined that the isotherm and streamline contours are rather insensitive to the actual shape of the energy generation rate function although their magnitudes are affected. The linear-positive-slope profile produced the coolest annulus and consequently the one circulating the most slowly. This is characteristic of profiles which peak near the outer sphere. The local wall heat flux results show that the northern regions of the outer sphere are subject to the major thermal stress. On the inner sphere, the northern latitudes are also the hottest.

REFERENCES

1. J. Nelsen, R. Douglass and D. Alexander, Natural convection in a spherical annulus filled with heat generating fluid, *Proc. 7th Int. Heat Transfer Conf.*, Vol. 2, pp. 171–176 (1982).
2. J. Nelsen, Natural convection of heat generating fluid in spherical annuli, M.S. thesis, University of Nebraska, Lincoln, Nebraska (1981).
3. J. M. Nelsen and R. W. Douglass, On partial spectral expansions using natural convection in spherical annulus enclosures as an example, *Numerical Heat Transfer* **6**, 67–84 (1983).

Int. J. Heat Mass Transfer. Vol. 27, No. 10, pp. 1928–1932, 1984
Printed in Great Britain

0017-9310/84 $3.00 + 0.00

Transport from a vertical ice surface melting in saline water

R. S. JOHNSON
Harrison Radiator Division, General Motors Corporation, Lockport, NY 14094, U.S.A.

and

J. C. MOLLENDORF
Mechanical and Aerospace Engineering, State University of New York at Buffalo, Amherst, NY 14260, U.S.A.

(*Received* 9 *February* 1983 *and in revised form* 20 *January* 1984)

INTRODUCTION

THE IMPORTANCE of ice–seawater interactions has been evident since the early investigation of Sandström [1]. Later, Neshyba [2] suggested that the upwelling produced by melting icebergs could strongly influence the supply of nutrients to Antarctic surface waters.

In saline water, the coupled effects of thermal and saline diffusion, on the motion-causing buoyancy force, results in considerable added complexity. Previous work dealing with the melting of ice in pure water has been summarized by Carey and Gebhart [3, 4], and includes abstracts of papers presented at meetings by Josberger and Martin [5] and Josberger [6] who have considered the buoyancy-induced flow near ice in seawater. In a more complete discussion of their work, Josberger [7, 8] and Josberger and Martin [9] report observations regarding vertical ice slabs melting in sea water. It was observed that next to the ice surface, upwardly flowing fluid began as laminar then developed into turbulence, where the transition location was governed by a saline Grashof number. Also, in the laminar regime, they observed bidirectional flow, with an upward inner flow and downward outer flow. They presented measured interface temperatures found by freezing themistors in the ice, but the effect of internal heat conduction in the ice is not clear. Strikingly increased local melting rates were observed in the transition region where the flow went from a bidirectional laminar flow to an upward turbulent flow. In this region, a 'notch' was formed in the ice as the entrained fluid divided to feed the upward and downward flows. Such a 'notch' was also seen in the work reported by Sandstrom [1].

Marschall [10] solved the boundary-layer equations governing heat, mass and momentum transfer and presented results for the relationships between interface temperature, ambient temperatures and interface salinity.

Carey and Gebhart [3, 4] numerically computed boundary-layer flow and transport adjacent to a vertical ice surface in saline water for a wide range of ambient salinities and temperatures. Their calculations show excellent agreement with the results of Josberger [8] and those from the present paper. They also conducted vertical ice melting experiments in $10^{\circ}/_{\circ\circ}$ saline water over the ambient temperature range of 1–15°C and showed, by a time exposure photographic technique, the nature of the natural convection flows.

EXPERIMENTAL APPARATUS AND PROCEDURE

Nominally, the present experiment consisted of melting a vertical, bubble-free ice slab of dimensions 30.3 cm high by 14.8 cm wide with an initial thickness of 3 cm in saline water at a concentration of about $35^{\circ}/_{\circ\circ}$. The actual ambient salinity ranged between 34.5 and $35.5^{\circ}/_{\circ\circ}$.

Frozen in the ice slab were five thermocouples to both measure the ice–liquid interface temperature, t_{il}, during melting; and, before a run, to determine when the entire slab was at the t_{il} temperature expected to result for the given ambient temperature. Equilibrium was obtained by 'over-freezing' the ice to a temperature below the expected t_{il} temperature for each individual experimental run. The ice was then put into an insulated box and allowed to warm slowly to the expected t_{il}. This procedure insured negligible internal conduction and consequently a very accurate inference of the interfacial melting temperature. This is necessary, since it would be difficult to separate out transient internal conduction effects accurately.